

# A constrained neural network model for soil liquefaction assessment with global applicability

Yifan ZHANG, Rui WANG\*, Jian-Min ZHANG, Jianhong ZHANG

*Department of Hydraulic Engineering, State Key Laboratory of Hydrosience and Engineering, Tsinghua University, Beijing 100084, China*

*\*Corresponding author. E-mail: wangrui\_05@mail.tsinghua.edu.cn*

© Higher Education Press 2020

**ABSTRACT** A constrained back propagation neural network (C-BPNN) model for standard penetration test based soil liquefaction assessment with global applicability is developed, incorporating existing knowledge for liquefaction triggering mechanism and empirical relationships. For its development and validation, a comprehensive liquefaction data set is compiled, covering more than 600 liquefaction sites from 36 earthquakes in 10 countries over 50 years with 13 complete information entries. The C-BPNN model design procedure for liquefaction assessment is established by considering appropriate constraints, input data selection, and computation and calibration procedures. Existing empirical relationships for overburden correction and fines content adjustment are shown to be able to improve the prediction success rate of the neural network model, and are thus adopted as constraints for the C-BPNN model. The effectiveness of the C-BPNN method is validated using the liquefaction data set and compared with that of several liquefaction assessment methods currently adopted in engineering practice. The C-BPNN liquefaction model is shown to have improved prediction accuracy and high global adaptability.

**KEYWORDS** soil liquefaction assessment, case history dataset, constrained neural network model, existing knowledge

## 1 Introduction

Consequences of soil liquefaction, such as sand boiling and ejecta, loss of soil strength, lateral spreading, and ground settlement and upheaval, are a major source of seismic hazard [1–4]. Accurate assessment and prediction of liquefaction is an important issue in geotechnical engineering, especially in seismically active areas. Standard penetration tests (SPT) have long been used to develop various prediction methods based on liquefaction case histories. Although recent developments in cone penetration test (CPT) technology has promoted its use in liquefaction assessment [5,6], SPT is still widely used in many parts of the world due to its simplicity, cost efficiency, and accumulation of historic data [7,8], especially in China and Japan. SPT based liquefaction assessment methods can generally be divided into two categories: traditional simplified semi-empirical methods,

including the liquefaction cyclic resistance method [9,10], the liquefaction safety factor method [11–13], and the critical SPT- $N$  method [14,15]; data-driven statistical and machine learning methods, such as artificial neural network methods [16,17], decision tree methods [18], support vector machine methods [19,20], and logistic regression methods [21–23]. Data-driven methods are more effective in establishing complicated nonlinear relationships between liquefaction and various factors, and can provide more effective use of available data.

Currently, one limitation of existing data-driven methods is that they have mostly been derived from a single earthquake event or very limited number of earthquakes, lacking more general validation and application [18,19,22]. While there are several existing SPT liquefaction data sets, the application of these data sets in developing highly adaptable data-driven liquefaction assessment methods need to resolve issues related to consistency of parameter selection and data coverage. For example, current datasets used in various regions are often

highly biased in data origin and could lead to applicability issues when used in different regions, restricting their global adaptability [24–26]. Recently, there have been several collaborative efforts in developing liquefaction related databases, including the Next-Generation Liquefaction (NGL) [27,28] and the “LiqChina” liquefaction case history database [29].

Within the data-driven methods, use of back propagation neural network (BPNN) has high application potential for liquefaction assessment with strong learning ability, high classification accuracy, and sufficient approximation for complex nonlinear relationships [30–32]. However, the prediction accuracy and consistency of existing BPNN liquefaction assessment methods are significantly limited by data selection and parameter calibration. For instance, the data used for liquefaction manifestation prediction and model training are often from the same origin and limits the evaluation of the true predictive power of the methods [33,35]. The neural network design procedure and determination of model parameters often rely heavily on experience [35]. In addition, well established understandings of liquefaction triggering mechanism and empirical relationships are not fully utilized [15,33,34]. It has been shown that incorporation of prior knowledge in neural networks can improve its performance, often referred to as feature engineering [36–39]. One way of incorporating prior knowledge in neural networks is as constraints during input to guide the training process, and has been proven to be effective [40].

This study aims to establish a globally applicable constrained back propagation neural network (C-BPNN) model for SPT based soil liquefaction assessment, incorporating considerations for liquefaction triggering mechanism and empirical relationships. A comprehensive liquefaction data set for neural network training, validation, and evaluation is compiled, covering more than 600 liquefaction sites from 36 earthquakes in 10 countries over 50 years with 13 information entries. A C-BPNN model design procedure for liquefaction assessment is developed by considering appropriate constraints, input, and computation and calibration procedures. The adaptability of the C-BPNN method in various regions of the world is validated using the compiled liquefaction data set and compared with that of several liquefaction assessment methods widely adopted in engineering practice.

## 2 Compilation of a comprehensive liquefaction case history SPT data set

To develop a high adaptability data-driven SPT based liquefaction assessment method, a comprehensive liquefaction case history SPT data set is first compiled. Several data sets have been compiled in the past for liquefaction

assessment, including Cetin et al. [24], Boulanger and Idriss [41], Idriss and Boulanger [25], and Xie [42], which are adopted and merged in this study to form the basics of the current data set. Liquefaction case history data from several major earthquakes from the past two decades are also gathered and added to the data set, mainly including the 1999 Chi-Chi earthquake [8,43], the 1999 Kocaeli earthquake [44,45], the 2003 Bachu earthquake [46,47], the 2010 Haiti earthquake [48–50], the 2010 Chile earthquake [7,51–53], and the 2011 Tohoku earthquake [54–56].

Thirteen data entries are collected for each site, including: earthquake magnitude ( $M_w$ ), earthquake type ( $ET$ ), peak ground acceleration ( $a_{max}$ ), critical depth ( $d_s$ ), groundwater level ( $d_w$ ), effective stress ( $\sigma'_v$ ), total stress ( $\sigma_v$ ), SPT value (SPT- $N$ ), fines content ( $FC$ ), clay content ( $CC$ ), average particle size ( $D_{50}$ ), soil type ( $ST$ ), and whether liquefaction manifestation occurs. The earthquake type ( $ET$ ) considers combinations of earthquake mechanism (intraplate earthquakes, interplate earthquakes, and subduction-zone earthquakes) and time distribution (isolated-shock, double-shock, main-shock, and multi-shock). Soil types ( $ST$ ) include clean sands ( $S$ ), sands with fines ( $SF$ ), silty sands, sand-silt mixture ( $SM$ ) and silts and very fine sands, silty of clayey fine sands or clayey silts with slight plasticity ( $ML$ ). The liquefaction critical layer at each site is determined as the layer of liquefiable soil type, within the immediate vicinity of the minimum SPT- $N$  value where SPT- $N$  values do not exceed 1.5 times that of the minimum value.

When compiling the data set, case histories with more than two missing data entries are eliminated, the missing entries for each site is completed using the random forest algorithm [57]. When using the random forest algorithm, the data without the missing entry are used in training for prediction, and the input entries are all transformed into numbers following the description in Fig. 1 and normalized. The number of trees, node size, and split are optimized for best performance. Note that  $(N_1)_{60}$  is not available in the data set of Xie [42]. Thus,  $N_1$  is used here as an approximation to  $(N_1)_{60}$ . A comprehensive liquefaction data set covering more than 600 liquefaction sites from 36 earthquakes in 10 countries over 50 years is ultimately established, with Table 1 showing an overview of the data set.

Compared with existing liquefaction data sets commonly used in liquefaction assessment [24,25,41,42], the data set compiled in this study expands in data volume and coverage, evident from Table 2. The number of liquefaction case histories in this data set is 2–3 times that of existing liquefaction data sets. The number of data entries is increased to 13, from 9 or 10. There is a noticeable expansion in the data coverage, especially for the critical depth, cyclic stress ratio and earthquake magnitude. In

**Table 1** An overview of the liquefaction data set compiled in this study

label	year	country	earthquake	number		
				all <sup>a)</sup>	liq <sup>b)</sup>	non-liq <sup>c)</sup>
1	1962	China	Heyuan	1	0	1
2	1966		Xingtai (Mar 8)	8	4	4
3	1966		Xingtai (Mar 22)	7	7	0
4	1967		Hejian	2	2	0
5	1969		Bohai	5	5	0
6	1969		Yangjiang	4	3	1
7	1970		Tonghai	32	17	15
8	1975		Haicheng	16	10	6
9	1976		Tangshan	99	60	39
10	1999		Chi-Chi	82	55	27
11	2003		Bachu	47	21	25
12	1944	Japan	Tohnankai	3	3	0
13	1948		Fukui	2	2	0
14	1964		Niigata	12	8	4
15	1968		Hososhima	1	0	1
16	1968		Tokachi-Oki	5	3	2
17	1978		Miyagiken-Oki (Feb 20)	14	1	13
18	1978		Miyagiken-Oki (Jun 12)	20	14	6
19	1980		Mid-Chiba	2	0	2
20	1982		Urakawa-Oki	1	0	1
21	1983		Nihonkai-Chubu	32	17	15
22	1984		Hososhima	1	0	1
23	1995		Kobe	54	25	29
24	2011		Tohoku	55	49	6
25	1971	USA	San Fernando	2	2	0
26	1979		Imperial Vally	9	4	5
27	1987		Superstition Hills	12	1	11
28	1989		Loma Prieta	25	16	9
29	1994		Northridge	4	3	1
30	1976	Guatemala	Guatemala	3	2	1
31	1977	Argentina	Argentina	5	3	2
32	1981	Britain	West Morland	7	3	4
33	1990	Philippines	Luzon	3	2	1
34	1999	Turkey	Kocaeli	14	12	2
35	2010	Haiti	Haiti	13	11	2
36	2010	Chile	Chile	15	12	3
total				617	377	240

Note: a) all = all cases including liquefaction and non-liquefaction sites; b) liq = liquefaction sites; c) non-liq = non-liquefaction sites.

addition, some liquefaction case histories with critical depth less than 2 m or more than 15 m, fines content over 35% (non-plastic), and magnitude over 7.8 are added through additional data from recent earthquakes. Comparison of the data source regional distribution in various data sets shows the new data set has a wider distribution with emphasis on Chinese case histories. The datasets of Cetin 00 [24] and BI 14 [41] are mostly from Japan and USA and have very few data points from China, while the data in Xie 84 [42] is mostly from China with limited coverage of USA case histories. Therefore, use of the dataset compiled in this study is expected to improve the global adaptability of the outcome liquefaction assessment method.

The distribution of each data entry within the data set is elaborately illustrated in Fig. 1. In regard to seismic conditions, the magnitude distributes in the range of  $M_w = 5.9-9.0$ , over 80% are within 6.5–8.0, suggesting that although earthquakes with smaller magnitude are more frequent, they cause fewer cases of liquefaction manifestation. The peak ground acceleration ranges from 0.05g to 0.84g, among which  $a_{\max} = 0.15g-0.40g$  are the main components. The critical depth, groundwater level, effective stress and total stress in the data set distribution follow lognormal type patterns, and distribute within 0.5–23.5 m, 0–9.6 m, 4.0–230.4 kPa, and 6.37–374.4 kPa, respectively, with liquefaction mostly occurring in middle and shallow layers at critical depth of 1–8 m and groundwater level of 0–3 m. SPT- $N$  value ranges from 1 to 99, and also exhibit lognormal distribution patterns. Fines content ranges from 0 to 96%, clay content ranges from 1 to 18%, and average particle size ranges from 0.015 to 2.4 mm in the data set. Liquefiable soils are mainly clean sand and silty fine sand with SPT- $N$  value smaller than 20, and fines content are mostly less than 50%.

### 3 C-BPNN model for liquefaction assessment

#### 3.1 Basic concept of the C-BPNN model

BPNN is a computational network based on error back propagation algorithm, which consists of neurons that interact with each other through weighted interconnections between three main network layers: the input, hidden and output layers [30,32,58].

A C-BPNN model (Fig. 2) is established in this study based on BPNN, to take into consideration existing knowledge for liquefaction triggering mechanism and empirical relationships. Existing knowledge is incorporated in the input layer along with the usual input data in the C-BPNN model, constraining the relationship established by the neural network. Here, input entries are derived from in situ test, and they are the most basic physical factors influencing liquefaction triggering, whereas constraints are relationships of input entries, which are derived from laboratory tests and practical experience. In the C-BPNN model, the optimization of input entries is separate from the optimization of constraints. The basic physical factors are first evaluated to obtain the optimal input entries, after which, constraints based on existing knowledge are introduced and evaluated to improve model performance. For example, one may choose to use equivalent clean sand adjustment  $\Delta(N_1)_{60}$  determined from existing empirical relations as a constraint to reflect the effect of non-plastic fines.

#### 3.2 Model computation procedure

The effectiveness of C-BPNN model is influenced by the

**Table 2** Comparison between the data set in this study and three existing data sets

data sets	Cetin 00	BI 14	Xie 84	this paper
liquefaction cases	109	135	125	377
non-liquefaction cases	88	115	76	240
data entries	9	10	9	13
critical depth (m)	1.1–20.5	1.8–14.3	0.5–18.5	0.5–23.5
effective stress (kPa)	8.1–198.7	20.3–170.9	4.3–185.5	4.0–230.4
fines content (%)	0–92	0–92	–	0–96
$N_1$ (60cs)	2.2–66.1	4.6–63.7	1.4–66.0	1–69
cyclic stress ratio	0.05–0.66	0.04–0.69	0.04–0.78	0.03–0.84
magnitude	5.9–8.0	5.9–8.3	6.3–7.8	5.9–9.0
data sources				
China	9	21	174	303
Japan	144	147	24	202
USA	39	50	3	52
others	5	32	0	60

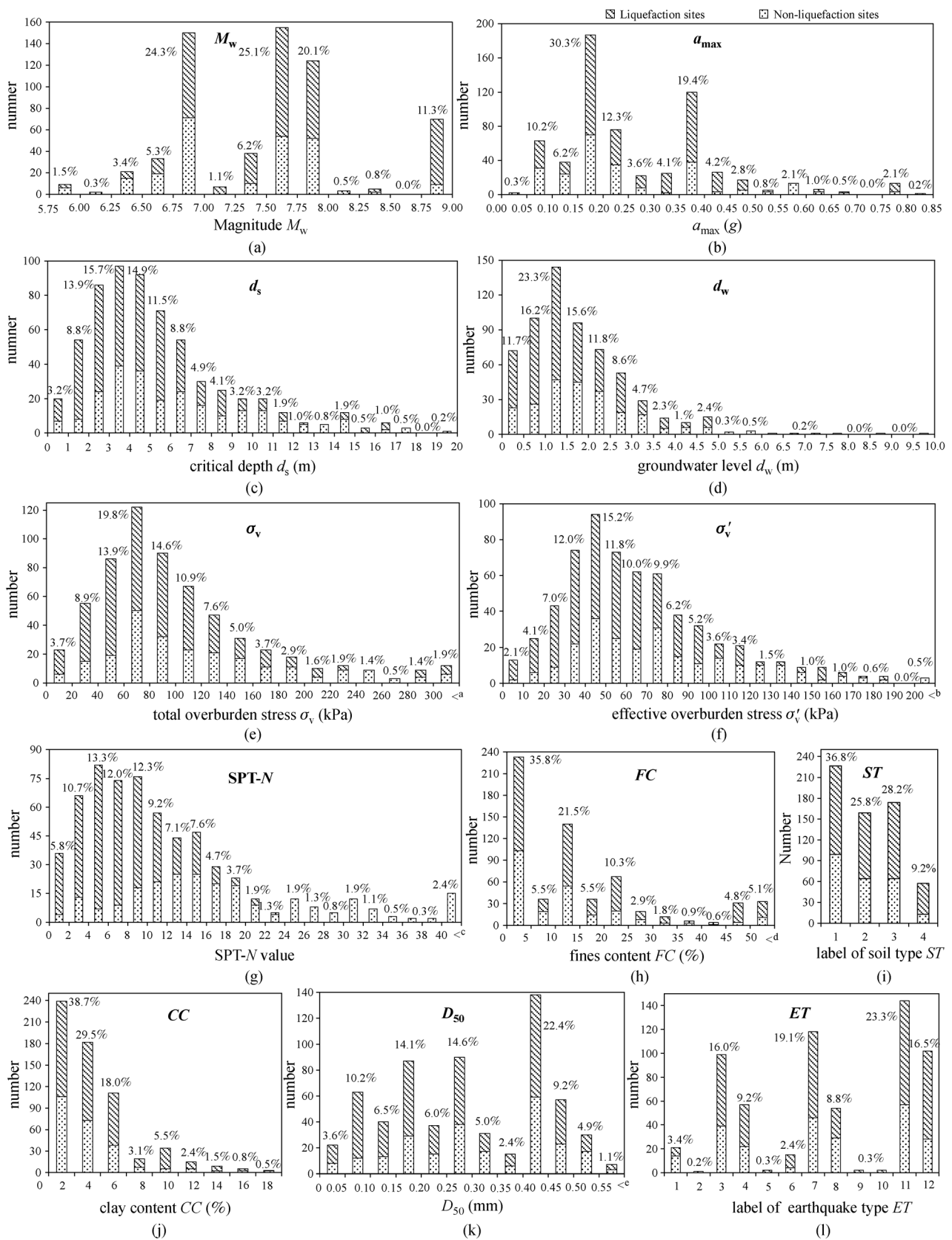


**Fig. 1** Data distribution of each information entry: (a)  $M_w$ ; (b)  $a_{max}$ ; (c)  $d_s$ ; (d)  $d_w$ ; (e)  $\sigma_v$ ; (f)  $\sigma'_v$ ; (g) SPT-N; (h) FC; (i) ST; (j) CC; (k)  $D_{50}$ ; (l) ET. Note: 1) Soil types (ST) include clean sands (1-S), sands with fines (2-SF), silty sands, sand-silt mixture (3-SM), and silts and very fine sands, silty of clayey fine sands or clayey silts with slight plasticity (4-ML); 2) Earthquake type (ET) include combinations of various earthquake mechanisms (1-intraplate earthquakes, 2-interplate earthquakes and 3-subduction-zone earthquakes) and time distributions (1-isolated-shock, 2-double-shock, 3-main-shock, and 4-multi-shock). The correspondence of labels in Fig. 1(l) with earthquake mechanisms and time distributions are: 1 = 1-1, 2 = 1-2, 3 = 1-3, 4 = 1-4; 5 = 2-1, 6 = 2-2, 7 = 2-3; 8 = 2-4; 9 = 3-1, 10 = 3-2, 11 = 3-3, 12 = 3-4. 3. ' $<^a$ ', in (e) indicates  $\sigma_v > 300$  kPa, ' $<^b$ ', in (f) indicates  $\sigma'_v > 200$  kPa, ' $<^c$ ', in (g) indicates SPT-N  $> 40$ , ' $<^d$ ', in (h) indicates FC  $> 50\%$ , and ' $<^e$ ', in (k) indicates  $D_{50} > 0.55$  mm.

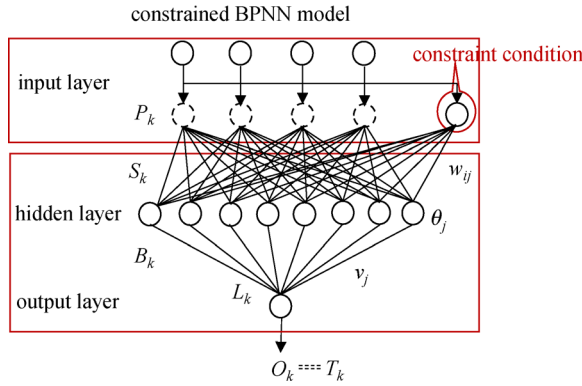


**Fig. 2** Structure of the constrained BPNN (C-BPNN) model. Note:  $P_k$  is the input data,  $T_k$  is the target output,  $S_k$  and  $B_k$  are the input and output of hidden layer,  $L_k$  and  $O_k$  are the input and output of output layer, where  $k$  is the label of input sample with  $k = 1, 2, \dots, m$ , and  $m$  is the number of input samples.  $w_{ij}$ ,  $\theta_j$ ,  $v_j$ ,  $\gamma$  ( $i = 1, 2, \dots, n$ ,  $j = 1, 2, \dots, p$ ) are the connection weights and thresholds of input-hidden layer and hidden-output layer, respectively, where  $n$  is the number of input entries and  $p$  is the number of hidden neurons.

architecture layout, output function, and learning algorithm. The architecture layout is determined by the number of layers and the number of neurons in each layer. A three-layer model with one output is adopted here in accordance to existing studies [19,33,35]. The number of neurons in the input layer depends on the number of input data entries, and the number of neurons in the hidden layer is a parameter that requires determination. Three types of activation function can be used in the output layer: Log-Sigmoid, Tan-Sigmoid or Purelin [30]. Log-Sigmoid function is adopted, with output value within the range of 0–1, concentrated mainly at 0 and 1, where 0 corresponds to non-liquefaction and 1 corresponds to liquefaction.

To improve the training efficiency and ensure the best learning rate during the network training process, a self-adaptive adjustment learning rate algorithm is adopted based on a batch gradient descent (BGD) method [59,60]. A momentum term is also introduced in order to orient the error objective function gradient to the center of the error surface [60,61].

The computation procedure for the C-BPNN liquefaction assessment model is established as follows.

1) Input sample matrix  $\mathbf{P} = (\mathbf{P}_1, \dots, \mathbf{P}_k, \dots, \mathbf{P}_m)$  (including constraint conditions) and corresponding target output sample  $\mathbf{T} = (t_1, \dots, t_k, \dots, t_m)$  are provided to the network with  $\mathbf{P}_k = (a_1, a_2, \dots, a_n)$  and  $\mathbf{T}_k = (t_k)$  being the input and output of the  $k$ th sample, where  $m$  is the number of input samples and  $n$  is the number of input data entries.

2) The inputs  $\mathbf{S}_k = (s_1, s_2, \dots, s_p)$ ,  $\mathbf{L}_k = (l)$  and outputs  $\mathbf{B}_k = (b_1, b_2, \dots, b_p)$ ,  $\mathbf{O}_k = (o)$  of the hidden and output

layers are calculated as:

$$s_j = \sum_{i=1}^n w_{ij} a_i - \theta_j, \quad b_j = f(s_j) = \text{logsig}(s_j),$$

$$l = \sum_{j=1}^p v_j b_j - \gamma, \quad o = f(l) = \text{logsig}(l), \quad (1)$$

where  $w_{ij}$ ,  $\theta_j$ , and  $v_j$ ,  $\gamma$  ( $i = 1, 2, \dots, n$ ,  $j = 1, 2, \dots, p$ , with  $p$  being the number of hidden neurons) are the connection weights and threshold values of input-hidden layer and output-hidden layer, respectively.

3) Error correction terms  $d^k$  and  $e_j^k$  in output layer and hidden layer can be determined through the following formula:

$$d^k = (t - o) \cdot o(1 - o),$$

$$e_j^k = d^k v_j \cdot b_j(1 - b_j), \quad (j = 1, 2, \dots, p) \quad (2)$$

4) The connection weights  $w_{ij}$ ,  $\theta_j$  and threshold values  $v_j$ ,  $\gamma$  are then corrected accordingly:

$$v_j(N+1) = v_j(N) + \alpha \cdot \frac{1}{m} \sum_{k=1}^m d^k \cdot b_j + \beta \cdot \Delta v_j(N),$$

$$\gamma(N+1) = \gamma(N) + \alpha \cdot \frac{1}{m} \sum_{k=1}^m d^k + \beta \cdot \Delta \gamma(N), \quad (3)$$

$$w_{ij}(N+1) = w_{ij}(N) + \alpha \cdot \frac{1}{m} \sum_{k=1}^m e_j^k \cdot a_i + \beta \cdot \Delta w_{ij}(N),$$

$$\theta_j(N+1) = \theta_j(N) + \alpha \cdot \frac{1}{m} \sum_{k=1}^m e_j^k + \beta \cdot \Delta \theta_j(N),$$

where  $\alpha$  is the learning rate,  $\beta$  is the momentum factor, and  $N$  is the number of iteration step. The self-adaptive adjustment learning rate algorithm can be described as:

$$\alpha(N+1) = \begin{cases} 1.05 \cdot \alpha(N), & E(N+1) < E(N), \\ \alpha(N), & E(N) \leq E(N+1) \leq 1.04E(N), \\ 0.7 \cdot \alpha(N), & E(N+1) > 1.04E(N), \end{cases} \quad (4)$$

where  $E(N)$  is the global error after the  $N$ th iteration.

5) Process (1) to (4) is repeated for each sample.

6) Check for convergence determined by the error objective function. The network converges when the global error  $E$  is smaller than the error tolerance  $\varepsilon$ . If convergence is not achieved, iteration of process (1) to (6) is carried out.

Under this computation procedure, the design for the C-BPNN liquefaction assessment model requires considerations for model parameter selection, input data set selection, and constraint selection, which will be discussed in following subsections.

### 3.3 Model parameter selection

K-fold cross validation is adopted to determine the optimal model parameters. The input sample data  $P$  (learning samples other than test set) is evenly divided into 5 subsets, which are used 5 times to train and validate the C-BPNN model (Fig. 3). For each case in Fig. 3, 4 subsets are used as training sets while the remaining subset serves as the validation set. Subsequently, the model error  $E_{\text{general}}$  can be calculated by averaging the errors of all 5 cases ( $E_1, E_2, E_3, E_4, E_5$ ). The model parameters are hence chosen to minimize  $E_{\text{general}}$  value.

For the C-BPNN model, model parameters include the number of hidden neurons ( $p$ ), learning rate ( $\alpha$ ), and momentum factor ( $\beta$ ), for given error tolerance and iteration step values, which are here 1% and 10000, respectively. Hidden neuron number  $p$  ranging from 1 to 15, initial learning rate  $\alpha$  ranging from 0 to 1, and momentum factor  $\beta$  ranging from 0 to 1 are used to optimize the performance of the model. The prediction success rate ( $PSR$ ) is adopted to evaluate model performance, which is the number of correctly predicted sites, in terms of liquefaction manifestation or no liquefaction manifestation, divided by the number of sites [62]. The process of model parameter selection is presented here for a typical set of input layer data.

Figure 4 shows the influence of  $\beta$  value on  $PSR$  for various combinations of hidden neuron number ( $p$ ) and learning rate ( $\alpha$ ), for liquefaction sites, non-liquefaction sites, and all sites, respectively. The results show that the choice of momentum factors  $\beta$  has little influence on  $PSR$ , and thus a value of 0.9 is adopted in this study based on recommendation from previous studies [63].

Figure 5 shows the influence of learning rate  $\alpha$  on C-BPNN model performance ( $\beta = 0.9$ ). When  $\alpha$  is greater than 0.1, it has limited influence on model performance. When the learning rate is too small (i.e.,  $\alpha < 10^{-5}$ ), the model does not converge within 10000 iterations. The best model performance is achieved when  $\alpha$  is around 0.01.

The number of hidden neurons ( $p$ ) determines the structure of the model. The influence of  $p$  on model performance is shown in Fig. 6.  $E_{\text{general}}$  within 5% is achieved when  $p$  is between 5 and 9. Within  $p$  of 5 to 9, best overall  $PSR$  is achieved at  $p = 7$ .

### 3.4 Model input layer determination

The data and constraints used in the C-BPNN model ultimately determines its accuracy and adaptability. The input data set selection and constraint selection are discussed here. Note that both the input data sets and constraints are pre-processed by normalizing with z-score prior to the computation procedure [64].

#### 3.4.1 Input data set selection

The data set compiled in this study has 12 data entries for each site ( $M_w, a_{\text{max}}, ET, d_s, d_w, \sigma'_v, \sigma_v, \text{SPT-}N, FC, CC, D_{50}, ST$ ), excluding the information on whether liquefaction manifestation occurs, from 671 sites. The choice of data entry used as input data and sites used in model training is an important issue. Table 3 shows the three input entry combinations investigated in this study: the 8-entry combination covering basic information of seismic conditions, site conditions, and soil properties; the 11-entry combination with additional information for soil property; and the 12-entry combination incorporating earthquake type. A subset of sites selected as input sample data for training of the C-BPNN model (i.e., training set and validation set) is referred to a “basic dataset”, the rest of the data from the entire data set serve as “test dataset”. This sub-data set should be able to have good coverage of the overall characteristics of the entire liquefaction data set, with as few sites as possible. Five representative basic data sets with various important features (Table 4) are selected and compared.

Figure 7 compares the model performance for the input data sets with different input entry combinations and basic

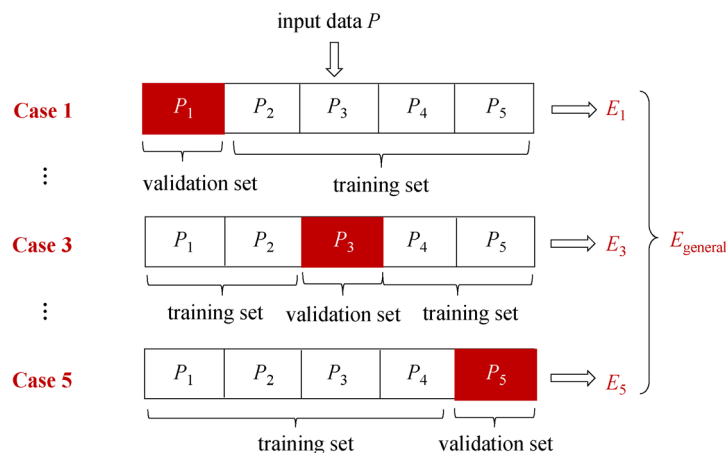
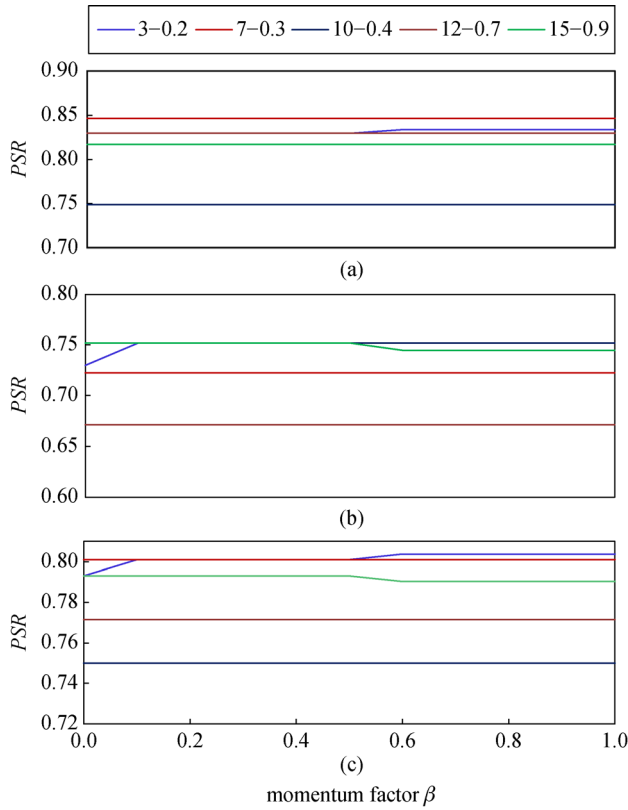


Fig. 3 Illustration of the process of 5-fold cross validation.



**Fig. 4** The influence of momentum factor  $\beta$  on C-BPNN liquefaction assessment model: (a)  $PSR$  in liquefaction sites; (b)  $PSR$  in non-liquefaction sites; (c)  $PSR$  in all sites. Note: The legend shows parameters of the computation models. For simplicity, the computation model with number of hidden neurons  $p = 3$  and learning rate  $\alpha = 0.2$  is abbreviated as 3-0.2 model.

data sets. The 8-entry combination for input data shows good overall performance. The extra information provided for the other two data entry combinations is not able to significantly and consistently improve the performance of the model, and may even hinder model performance in certain cases. For the 8-entry input data, basic data set-1 and basic data set-3 exhibit the highest overall  $PSR$ . Greater  $PSR$  is achieved for liquefaction sites using basic data set-3 while greater  $PSR$  is achieved for non-liquefaction sites using basic data set-1. Basic data set-3 has 55 more sites than basic data set-1, and there are 2.43 times as many liquefaction sites as non-liquefaction sites in basic data set-3. Therefore, considering the data amount and bias, the 8-entry basic data set-1 is selected for model training.

### 3.4.2 Constraint selection

Using the aforementioned input data entries alone does not allow for the incorporation of existing knowledge on liquefaction triggering in the neural network model. Accumulated knowledge from laboratory tests and empiri-

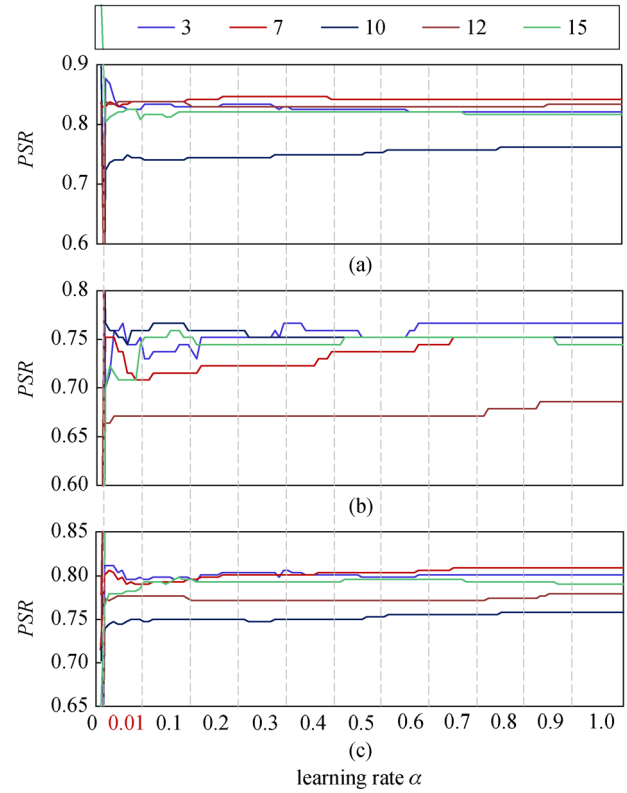


**Fig. 5** The influence of learning rate  $\alpha$  on C-BPNN liquefaction assessment model: (a)  $PSR$  in liquefaction sites; (b)  $PSR$  in non-liquefaction sites; (c)  $PSR$  in all sites. Note: The numbers in the legend indicate the number of hidden neurons.

cal relationships used in simplified liquefaction assessment methods [9,25,41,65–72] can potentially aid the performance of the model, which can be used as constraints in the model input layer. Five potential constraints are explored in this study, including: the stress reduction coefficient  $\gamma_d$ , the magnitude scaling factor  $MSF$ , the overburden correction factor  $K_s$ , the overburden correction factor  $C_N$ , and the equivalent clean sand adjustment  $\Delta(N_1)_{60}$ . The roles of these constraints are briefly described in the following, detailed formulations for these constraints can be found in each respective reference.

The stress reduction coefficient  $\gamma_d$  is used to adjust the maximum shear stress in soil for a site under a given earthquake motion, reflecting the deformability of soil [9]. It is suggested to be dependent on ground motion, shear wave velocity profile, and soil properties [65].

The magnitude scaling factor  $MSF$  is used to adjust the cyclic resistance of soil under any earthquake magnitude  $M_w$  [66], to that under  $M_w = 7.5$ . The  $MSF$  relationship adopted here is modified and revised by Boulanger and Idriss [41] based on currently available  $MSF$  relationships [67,68].

The overburden correction factor  $K_a$  is used to reflect the influence of effective overburden stress on the cyclic

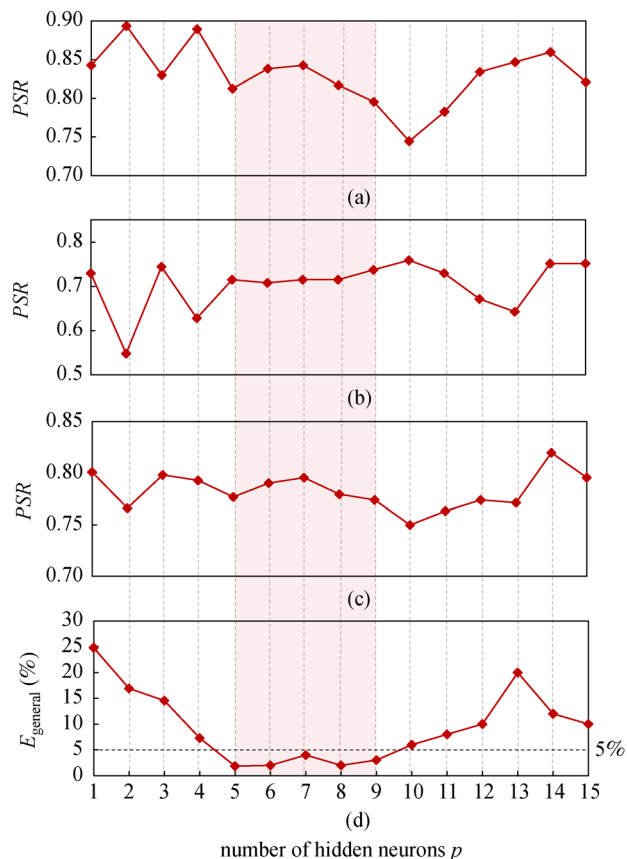


**Fig. 6** The influence of hidden neuron number  $p$  on C-BPNN liquefaction assessment model: (a)  $PSR$  in liquefaction sites; (b)  $PSR$  in non-liquefaction sites; (c)  $PSR$  in all sites; (d) the  $E_{\text{general}}$  of C-BPNN liquefaction assessment models with different hidden neuron number  $p$ .

**Table 3** Different combinations of input data entry

combinations	input entry	characteristics
8-entry	$M_w, a_{\text{max}}, d_s, d_w, \sigma_v, \sigma_v', N, FC$	basic information
11-entry	+ $D_{50}, CC, ST$	additional information for soil property
12-entry	+ ET	additional information for earthquake type

resistance of soil [66]. The relationship of  $K_s$  used here is developed by Cetin et al. [68] and Idriss and Boulanger [25].

SPT overburden correction factor  $C_N$  is introduced to normalize SPT- $N$  values under different vertical effective stress to an equivalent value at vertical effective stress of 101 kPa [66]. A number of different  $C_N$  relationships have been derived from SPT calibration chamber test results and field data [25,69–71], and the relationship recommended by Idriss and Boulanger [25] is adopted here.

Equivalent clean sand adjustment  $\Delta(N_1)_{60}$  is used to

adjust the SPT blow count  $N$  to that of clean sand with consideration for the effects of fines content [25].  $\Delta(N_1)_{60}$  expression developed by Idriss and Boulanger [25] is adopted here, which has been examined using data from recent earthquakes [41,65].

Evaluation of the effectiveness of the different constraints is conducted by implementing each alone or in combination into the model. For generality, both the optimal input data set 8-1 (8-entry basic data set-1) and the input data set 8-3 (8-entry basic data set-3) are applied for this evaluation process. The  $PSR$  for each scenario is shown in Fig. 8, for liquefaction sites, non-liquefaction sites, and all sites.

For both input data sets, constraints  $C_N$  and  $\Delta(N_1)_{60}$  can improved the prediction ability of the model to some extent, in comparison to the case where no constraints are used.  $\gamma_d, MSF,$  and  $K_s$  are shown to have mixed effects, resulting in general in a lower overall  $PSR$ . Therefore, the combined effect of overburden correction factor  $C_N$  and equivalent clean sand adjustment  $\Delta(N_1)_{60}$  is further explored (Fig. 8). For input data set 8-1, a combination of  $C_N$  and  $\Delta(N_1)_{60}$  can further enhanced the  $PSR$ , for which  $C_N$  facilitates improved prediction performance in non-liquefaction sites and  $\Delta(N_1)_{60}$  contributes to improved prediction performance in liquefaction sites. It is worth noting that,  $\Delta(N_1)_{60}$  cannot replace the original input entry  $FC$ . If  $\Delta(N_1)_{60}$  is used to replace the original input entry  $FC$  instead of supplementing input, the overall  $PSR$  decreases significantly from 0.83 to 0.75.

Through the selection of model parameter, input data set, and constraint condition, a 3-layer 7-hidden neuron C-BPNN model with momentum factor of 0.9, learning rate of 0.01 is established using an 8-entry basic data set-1 with  $C_N$  and  $\Delta(N_1)_{60}$  as constraints for the final model.

## 4 Evaluation of the C-BPNN liquefaction assessment model

### 4.1 Validation on a global scale

To validate the effectiveness of the C-BPNN model developed in this study, it is used to conduct liquefaction assessment for the entire data set compiled in Section 2. Its performance is compared with that of several existing liquefaction assessment methods commonly used in engineering practice in various regions in the world, including: a) the code for seismic design of buildings method in China (CSDB01 and CSDB10) [73,74]; b) the Tokimatsu and Yoshimi (T-Y) method [75] and the Japan Road Association (JRA) method [13] in Japan; c) the NCEER method [76] and Boulanger-Idriss (B-I14) method [41] in USA.

Figure 9 shows the prediction results for all of the liquefaction case histories in the data set compiled in this

**Table 4** Basic information and main characteristics of 5 different basic data sets

basic database	year	country	earthquake	main characteristics
1	1966	China	Xingtai (Mar 8)	shallow ground liquefaction with small earthquake magnitude
	1966	China	Xingtai (Mar 22)	shallow ground liquefaction with medium magnitude
	1976	China	Tangshan	medium ground liquefaction with large magnitude (right-beneath-city type earthquake)
	1978	Japan	Miyagiken-Okii (Feb 20)	medium ground liquefaction with small earthquake magnitude
	1978	Japan	Miyagiken-Okii (Jun 12)	medium ground liquefaction with medium earthquake magnitude
	1989	USA	Loma Prieta	medium ground liquefaction with small earthquake magnitude
	1994	USA	Northridge	deep ground liquefaction with large acceleration
	1995	Japan	Hyogoken-Nambu (Kobe)	gravel sand liquefaction with right-beneath-city type earthquake
	1999	Turkey	Kocaeli	high fines content
2	1968	Japan	basic data set-1 + Tokachi-Okii	shallow ground liquefaction with large earthquake magnitude
3	2011	Japan	basic data set-1 + Tohoku	abundant liquefaction case histories
4	1981	UK	basic data set-1 + West Morland	high fines content with small earthquake magnitude
5	1994	USA	basic data set-1-Northridge	deep ground liquefaction with large acceleration

study (Table 1) for these seven methods. In Fig. 9, the successfully predicted liquefaction and non-liquefaction sites and unsuccessfully predicted liquefaction and non-liquefaction sites are plotted in different shades of colors. For the six existing methods, the prediction results are significantly region biased. The T-Y, NCEER, and B-I14 methods show relatively good performance for the case histories from Japan and USA, while not performing well for case histories from China. The JRA method is conservative for almost all case histories, with high rate of unsuccessful predictions in non-liquefaction sites. Although the Chinese methods (CSDB01 and CSDB10) exhibit marginally better performance for Chinese case histories, they perform poorly for case histories from the rest of the world.

Compared with traditional methods (Fig. 9), the C-BPNN method dramatically improves liquefaction prediction capabilities on a global level. The prediction accuracy of the C-BPNN model for the Japanese and USA case histories are slightly better than that of the T-Y, NCEER, and B-I14 methods, while the prediction results are significantly better for Chinese case histories than all existing methods (an increased *PSR* by 13% compared to the average prediction of existing methods), illustrating the high global adaptability of the proposed method. Especially, liquefaction in the 1999 Chi-Chi earthquake (label 10) is poorly predicted by existing methods, but is much

better predicted using the proposed C-BPNN method.

The *PSR* for liquefaction sites, non-liquefaction sites, and all sites in the entire data set for the seven different liquefaction assessment methods are plotted in Fig. 10. It can be seen that the *PSR* for all sites is the highest for the C-BPNN method, reaching 85%, compared to 80% of the second highest B-I14 method and 73% of the lowest JRA method. The *PSR* for liquefaction sites of C-BPNN is slightly lower than only the JRA and CSDB-01 methods, at 89%, 97%, and 90%, respectively. The *PSR* for non-liquefaction sites is drastically improved by the C-BPNN method, reaching 78%, compared with 72% of the second highest NCEER method and 36% of the lowest JRA method. In general, the prediction accuracy has been greatly improved, and the *PSR* for non-liquefaction sites, all sites and liquefaction sites of C-BPNN are improved by 24%, 9%, and 1%, respectively, compared to the average prediction of existing methods. The results presented in Fig. 9 and Fig. 10 include the entire data set. If the basic data set used in training is eliminated, the overall *PSR* for all the remaining sites for the C-BPNN method is 84%, only slightly lower.

Note that numerical tests on different initial values of weight and threshold are also conducted, to verify that the model is not sensitive to initialization, for values within the range of  $-1$  to  $1$ . The model is also trained for many times, to verify that the results are consistent.

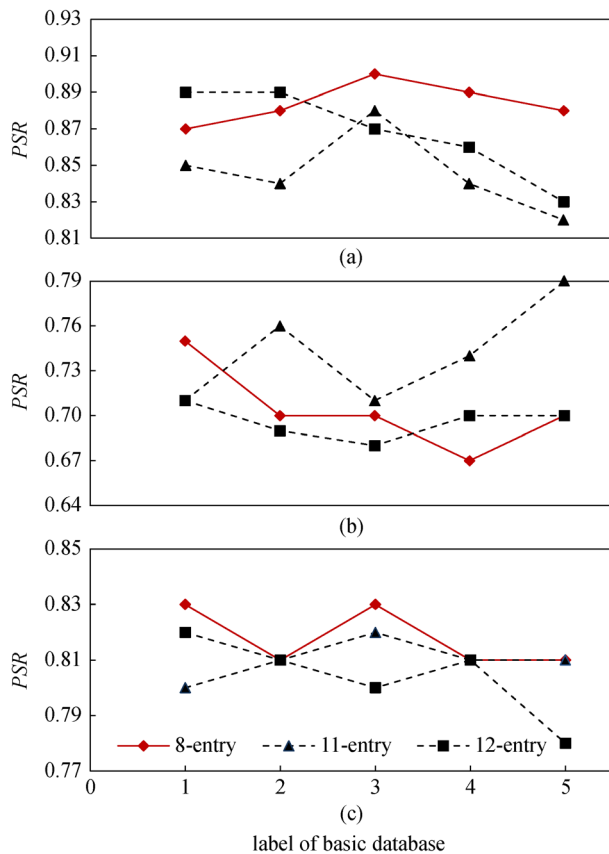


**Fig. 7** Input data set selection for C-BPNN liquefaction assessment method: (a)  $PSR$  in liquefaction sites; (b)  $PSR$  in non-liquefaction sites; (c)  $PSR$  in all sites.

#### 4.2 Validation for typical sites

Two typical boreholes from the 1999 Chi-Chi earthquake [43], which are not within the basic data set used to train the model, are selected as validations for typical sites for the C-BPNN method (Fig. 11). The Chi-Chi earthquake is a severe quake triggered by the rupture of a thrust fault with a magnitude ( $M_w$ ) of 7.6, and main shock that lasted approximately 40 s resulting in extensive liquefaction [7]. For site 1, liquefaction at a typical borehole in Nantou (Hole No. NT-BH-3) is predicted for peak ground acceleration of 0.428g. There are two potential liquefiable layer below groundwater level of 4 m: one is a medium dense silty fine sand layer between 3–9.2 m, and the other is a dense silty medium fine sand layer at 14–18 m. According to prediction results, the C-BPNN method successfully identified the first layer the liquefaction layer (Fig. 11(a)), consistent with the other existing methods, which has been confirmed during field investigation. Field investigation did not show conclusive results that liquefaction occurred in the second layer [7,41], and only the JRA and T-Y methods predict liquefaction in this layer.

For site 2, a typical borehole in a non-liquefaction site in

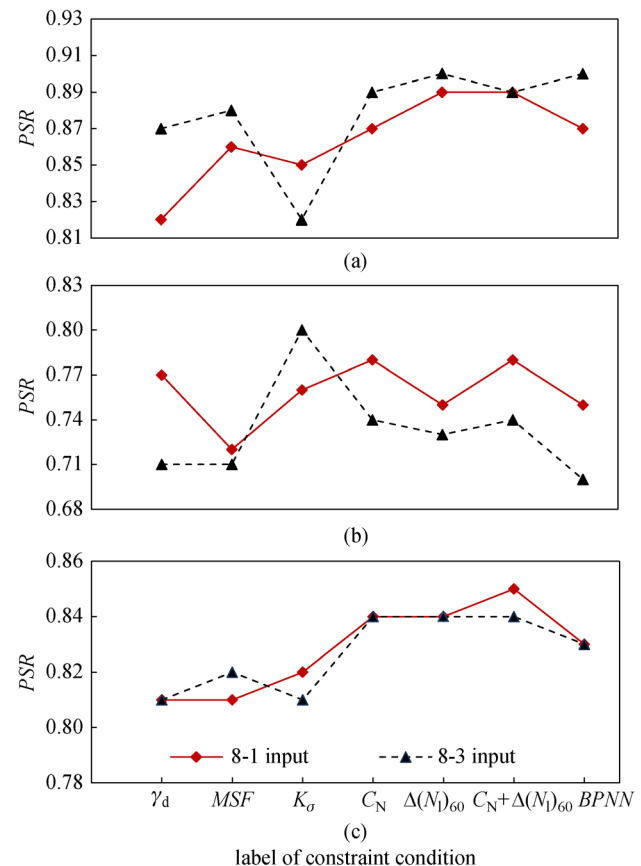


**Fig. 8** Constraint selection of C-BPNN liquefaction assessment method: (a)  $PSR$  in liquefaction sites; (b)  $PSR$  in non-liquefaction sites; (c)  $PSR$  in all sites. Note: BPNN on the  $x$ -coordinate refers to a model without any consideration of constraints.  $C_N + \Delta(N_1)_{60}$  indicates the combination of constraints  $C_N$  and  $\Delta(N_1)_{60}$ .

Wufeng (Hole No.WF-BH-8) is predicted under the peak ground acceleration of 0.789g. C-BPNN successfully identifies it as non-liquefaction site while all traditional methods identify the silty fine sand layer as a liquefaction layer (Fig. 11 (b)). Although there may be debate to whether liquefaction occurred at this site without manifestation [25], the prediction capability of the C-BPNN method for liquefaction manifestation is undoubted.

#### 4.3 Influence of various factors for liquefaction triggering

An advantage of the C-BPNN method is that it can be used to evaluate the contribution of various factors to liquefaction triggering through analysis of the weights for each model input. The factors considered here include: seismic conditions ( $M_w$ ,  $a_{max}$ ,  $ET$ ), site conditions ( $d_s$ ,  $d_w$ ,  $\sigma'_v$ ,  $\sigma_v$ ), and soil properties (SPT- $N$ ,  $FC$ ,  $CC$ ,  $D_{50}$ ,  $ST$ ), covering the 12 data entries in the data set. According to the weight distributions,  $w_i$  of different factors is calculated as expressed:



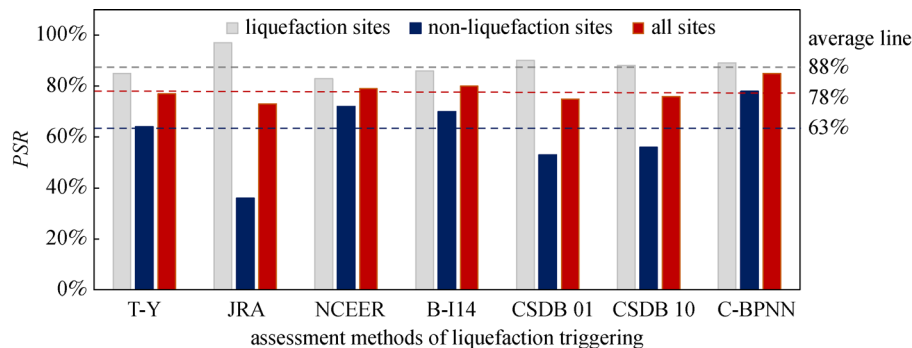


Fig. 10 Comparison of overall PSR of different liquefaction assessment methods.

$$w_i = \sum_{j=1}^n \left( v_j \times \left( w_{ij} / \sum_{i=1}^m w_{ij} \right) \right), \quad (5)$$

where  $w_{ij}$  and  $v_j$  are the connection weights of input-hidden layer and output-hidden layer, respectively, which are determined using the formulations in Section 3.2;  $i = 1, 2, \dots, m$ ,  $j = 1, 2, \dots, n$ ,  $m$  and  $n$  are the number of input neurons and hidden neurons, respectively.

The influence of various factors is analyzed using both the 8-entry combination and 12-entry combination for input data in Fig. 12. Soil properties are shown to be the most important factor affecting liquefaction triggering, with SPT- $N$  value having the greatest contribution. Seismic and site conditions show similar contributions to liquefaction triggering, with the peak ground acceleration  $a_{\max}$  a strongly influential factor. Site conditions of  $d_s$ ,  $d_w$ ,  $\sigma'_v$ , and  $\sigma_v$  have similar contributions of around 6%–8%. These findings are consistent with those by Hu et al. [77] based on a Bayesian network, where liquefaction is found to be most sensitive to soil properties.

## 5 Concluding remarks

Liquefaction assessment methods based on neural networks have a broad application prospect. This study tackled several limitations of existing neural network-based liquefaction assessment methods, including data bias and incompleteness, and the limited use of existing knowledge on liquefaction triggering. A C-BPNN liquefaction assessment model incorporating existing knowledge for liquefaction triggering mechanism and empirical relationships as appropriate constraints, based on a comprehensive global liquefaction data set was established.

A liquefaction data set covering more than 600 liquefaction sites from around the world, with 13 different information entries was compiled. Liquefaction case

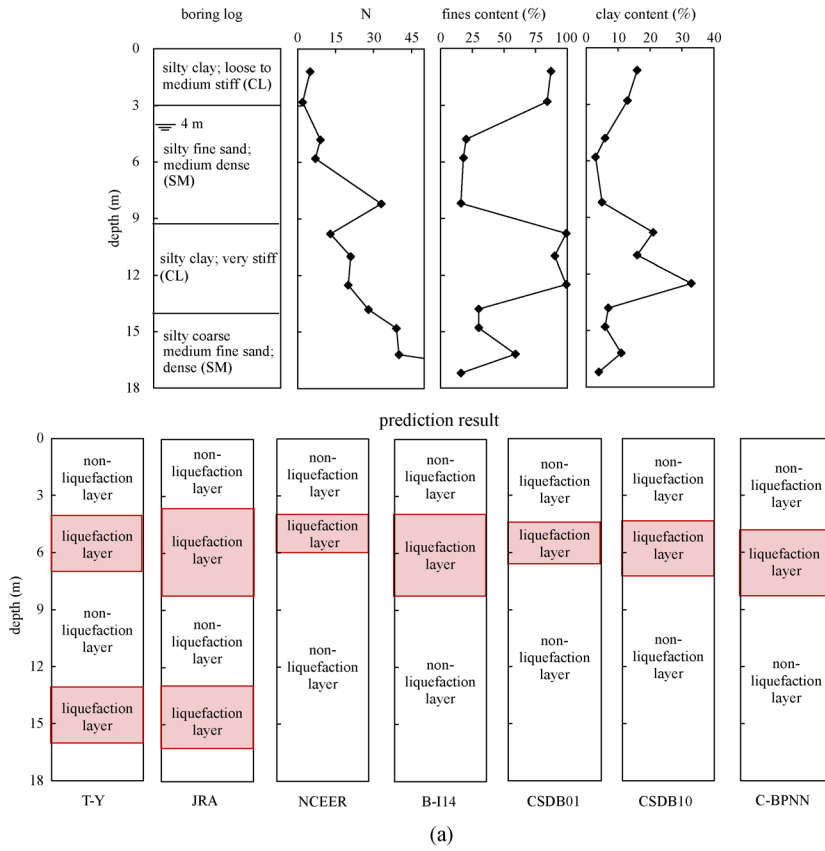
histories with critical depth less than 2 m or more than 15 m, fines contents over 35% and earthquake magnitude over 7.8 were added compared to existing data sets [24,41,42].

A design procedure of the C-BPNN model for liquefaction assessment was developed with consideration of constraints of  $\gamma_d$ ,  $MSF$ ,  $K_\alpha$ ,  $C_N$ , and  $\Delta(N_1)_{60}$ . A combination of K-fold cross validation algorithm for parameter selection and gradient descent method with self-adaptive adjustment learning rate  $\alpha$  and momentum factor  $\beta$  were applied in model construction, effectively resolving the problem of overfitting and local minimization. Analysis demonstrated that existing knowledge on liquefaction triggering can aid the performance of the neural network model. Constraints  $C_N$  and  $\Delta(N_1)_{60}$  can enhance model performance, and are thus incorporated.

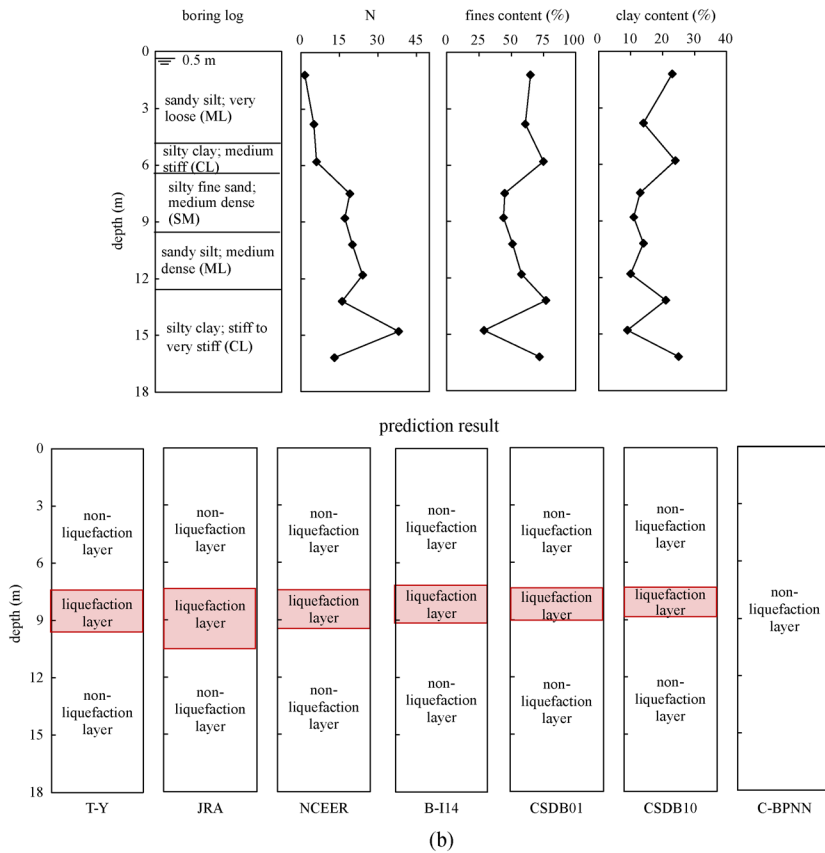
The effectiveness of the C-BPNN liquefaction assessment model was validated based on the comprehensively compiled data set, and is compared with several traditional methods commonly used in engineering practice. The C-BPNN method dramatically improved liquefaction prediction performance on a global level, compared with traditional methods which are significantly region biased [25,26]. The prediction accuracy of the C-BPNN liquefaction assessment model showed drastic improvements for prediction in non-liquefaction sites. Comparisons with typical borehole data further confirmed the effectiveness of the method.

Influence factors of liquefaction triggering were analyzed through comparing the weights for each model input. Liquefaction manifestation was shown to be most sensitive to soil properties, compared with earthquake and site conditions, similar to the conclusion drawn by Hu et al. [77] based on a Bayesian network.

Data-driven liquefaction assessment models, such as the one developed in this study, are inevitably based on liquefaction case history data. Currently, the proposed model is mainly restricted to clean sand and silty fine sand ( $FC \leq 50\%$ ) with critical depth no more than 23.5 m. However, the advantage of such models is that when new



(a)



(b)

**Fig. 11** Liquefaction assessment for two typical boreholes in the 1999 Chi-Chi earthquake using seven different methods (data derived from Juang [43]). (a) Site 1: Boring log, SPT-*N* value, fines content, clay content, and prediction results at a site in Nantou (Hole No. NT-BH-3) (Liq = Liquefaction); (b) Site 2: Boring log, SPT-*N* value, fines content, clay content, and prediction results at a site in Wufeng (Hole No. WF-BH-8) (Non-liq = Non-liquefaction).

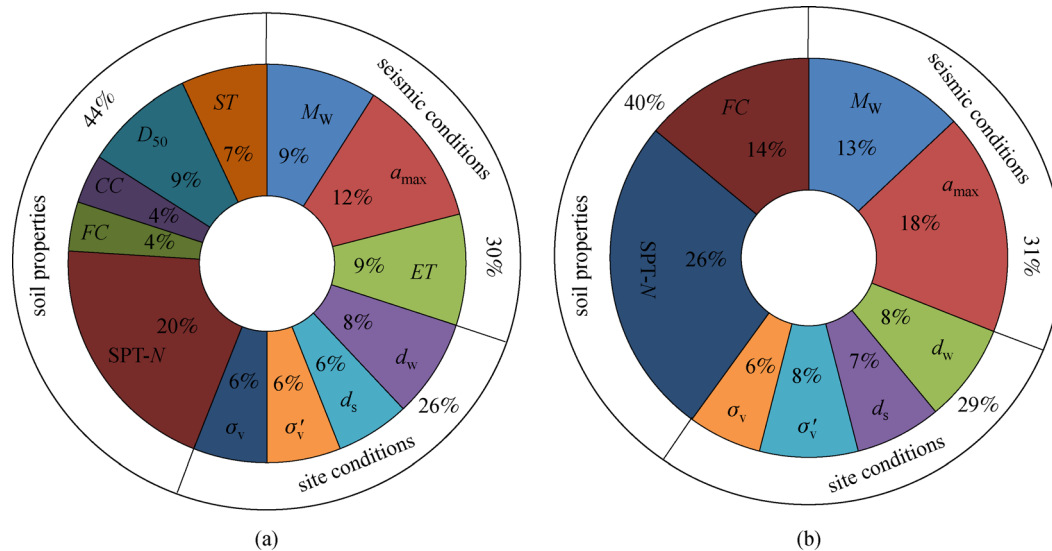


Fig. 12 Contribution of various factors influencing liquefaction triggering. (a) 12-entry combination; (b) 8-entry combination.

data becomes available, its incorporation into the models is straight forward.

**Acknowledgements** The authors would like to thank the National Natural Science Foundation of China (Grant Nos. 51678346 and 51879141) and Tsinghua University Initiative Scientific Research Program (2019Z08-QCX01) for funding this work.

## References

- Elgamal A W, Zeghal M, Parra E. Liquefaction of reclaimed island in Kobe. *Journal of Geotechnical and Geoenvironmental Engineering*, 1996, 122(1): 39–49
- Bardet J P, Mace N, Tobita T. Liquefaction-Induced Ground Deformation and Failure. Report to PEER/PG&E. 1999
- Sasaki Y, Towhata I, Miyamoto K, Shirato M, Narita A, Sasaki T, Sako S. Reconnaissance report on damage in and around river levees caused by the 2011 off the Pacific coast of Tohoku earthquake. *Soil and Foundation*, 2012, 52(5): 1016–1032
- Li Z Y, Yuan X M. Seismic damage summarization of site effect and soil liquefaction in 2016 Kaohsiung earthquake. *Earthquake Engineering and Engineering Dynamics*, 2016, 3: 1–7
- Robertson P K, Campanella R G. Liquefaction potential of sands using the CPT. *Journal of Geotechnical Engineering*, 1985, 111(3): 384–403
- Lees J J, Ballagh R H, Orense R P, van Ballegooy S. CPT-based analysis of liquefaction and re-liquefaction following the Canterbury earthquake sequence. *Soil Dynamics and Earthquake Engineering*, 2015, 79: 304–314
- Bray J D, Frost D. Geo-Engineering Reconnaissance of the February 27, 2010 Maule, Chile Earthquake. GEER Association Report No. GEER-022. 2010
- Chang M, Kuo C, Shau S, Hsu R. Comparison of SPT-N-based analysis methods in evaluation of liquefaction potential during the 1999 Chi-Chi earthquake in Taiwan. *Computers and Geotechnics*, 2011, 38(3): 393–406
- Seed H B. Simplified procedure for evaluating soil liquefaction potential. *Journal of the Soil Mechanics and Foundations*, 1971, 97(SM9): 1249–1273
- Bolton Seed H, Tokimatsu K, Harder L F, Chung R M. Influence of SPT procedures in soil liquefaction resistance evaluations. *Journal of Geotechnical Engineering*, 1985, 111(12): 1425–1445
- Ishihara K. Simplified method of analysis for liquefaction of sand deposits during earthquake. *Soil and Foundation*, 1977, 17(3): 1–17
- Tatsuoka F, Iwasaki T, Tokida K I, Yasuda S, Hirose M, Imai T, Kon-no M. Standard penetration tests and soil liquefaction potential evaluation. *Soil and Foundation*, 1980, 20(4): 95–111
- Japan Road Association. Specifications for Highway Bridges, Part V-Seismic Design. Tokyo: Japan Road Association, 2012
- State Infrastructure Commission. Code for Seismic Design of Industrial and Civil Buildings, TJ 11-74. Beijing: China Building Industry Press, 1974 (in Chinese)
- State Infrastructure Commission. Code for Seismic Design of Industrial and Civil Buildings, TJ 11-78. Beijing: China Building Industry Press, 1978 (in Chinese)
- Juang C H, Chen C J, Jiang T, Andrus R D. Risk-based liquefaction potential evaluation using standard penetration tests. *Canadian Geotechnical Journal*, 2000, 37(6): 1195–1208
- Zhang W G, Goh A T C. Assessment of soil liquefaction based on capacity energy concept and back-propagation neural networks. In: Samui P, Kim D, Ghosh C, eds. Integrating Disaster Science and Management, Global Case Studies in Mitigation and Recovery. Amsterdam: Elsevier, 2018: 41–51
- Gandomi H A, Fridline M M, Roke A D. Decision tree approach for soil liquefaction assessment. *The Scientific World Journal*, 2013, 2013: 1–8
- Goh A T C, Goh S H. Support vector machines: Their use in geotechnical engineering as illustrated using seismic liquefaction

- data. *Computers and Geotechnics*, 2007, 34(5): 410–421
20. Samui P. Least square support vector machine and relevance vector machine for evaluating seismic liquefaction potential using SPT. *Natural Hazards*, 2011, 59(2): 811–822
  21. Liao S S C, Veneziano D, Whitman R V. Regression models for evaluating liquefaction probability. *Journal of Geotechnical Engineering*, 1988, 114(4): 389–411
  22. Zhang W G, Goh A T C. Evaluating seismic liquefaction potential using multivariate adaptive regression splines and logistic regression. *Geomechanics and Engineering*, 2016, 10(3): 269–284
  23. Zhang J, Zhang L M, Huang H W. Evaluation of generalized linear models for soil liquefaction probability prediction. *Environmental Earth Sciences*, 2013, 68(7): 1925–1933
  24. Cetin K O, Seed R B, Moss R E S, Der Kiureghian A K, Tokimatsu K, Harder L F, Kayen R E. Field Performance Case Histories for SPT-Based Evaluation of Soil Liquefaction Triggering Hazard. Geotechnical Engineering Research Report No. UCB/GT-2000/09. 2000
  25. Idriss I M, Boulanger R W. *Soil Liquefaction During Earthquakes*. Oakland, CA: Earthquake Engineering Research Institute, 2008
  26. National Academy of Sciences. *State of the Art and Practice in the Assessment of Earthquake-Induced Soil Liquefaction and Its Consequences*. Washington, D.C.: National Academies Press, 2016
  27. Brandenberg S J, Kwak D Y, Zimmaro P, Bozorgnia Y, Kramer S L, Stewart J P. Next-Generation Liquefaction (NGL) Case History Database Structure. *Geotechnical Earthquake Engineering and Soil Dynamics V*, 2018, 290: 426–433
  28. Stewart J P, Kramer S L, Kwak D Y, Greenfield M W, Kayen R E, Tokimatsu K, Bray J D, Beyzaei C Z, Cubrinovski M, Sekiguchi T, Nakai S, Bozorgnia Y. PEER-NGL project: Open source global database and model development for the next-generation of liquefaction assessment procedures. *Soil Dynamics and Earthquake Engineering*, 2016, 91(SI): 317–328
  29. ISSMGE. 304dB TC304 databases. Extracted from the website of TC304 Engineering Practice of Risk Assessment & Management. 2019
  30. Rumelhart D E, Hinton G E, Williams R J. *Learning Internal Representations by Error Propagation*. Cambridge: MIT Press, 1986, 319–362
  31. Alsmadi M K S, Omar K B, Noah S A. Back propagation algorithm: The best algorithm among the multi-layer perceptron algorithm. *International Journal of Computer Science and Network Security*, 2009, 9(4): 378–383
  32. Nicoletti G M. An analysis of neural networks as simulators and emulators. *Cybernetics and Systems*, 2000, 31(3): 253–282
  33. Hanna M A, Ural D, Saygili G. Neural network model for liquefaction potential in soil deposits using Turkey and Taiwan earthquake data. *Soil Dynamics and Earthquake Engineering*, 2007, 27(6): 521–540
  34. Kumar V, Venkatesh K, Tiwari R P, Kumar Y. Application of ANN to predict liquefaction potential. *International Journal of Computational Engineering Research*, 2012, 2(2): 379–389
  35. Penumadu D, Goh A T C. Seismic liquefaction potential assessed by neural networks. *Journal of Geotechnical Engineering*, 1996, 122(4): 323–326
  36. Tresp V, Hollatz J, Ahmad S. Network structuring and training using rule-based knowledge. In: *Advances in Neural Information Processing Systems*. San Francisco, CA: Morgan-Kaufmann, 1993, 871–878
  37. Thompson M L, Kramer M A. Modeling chemical processes using prior knowledge and neural networks. *AICHE Journal. American Institute of Chemical Engineers*, 1994, 40(8): 1328–1340
  38. Wang F, Zhang Q J. Knowledge-based neural models for microwave design. *IEEE Transactions on Microwave Theory and Techniques*, 1997, 45(12): 2333–2343
  39. Nagarajan H P N, Mokhtarian H, Jafarian H, Dimassi S, Bakrani-Balani S, Hamed A, Coatanéa E, Gary Wang G, Haapala K R. Knowledge-based design of artificial neural network topology for additive manufacturing process modeling: A new approach and case study for fused deposition modeling. *Journal of Mechanical Design*, 2019, 141(2): 021705
  40. Han F, Huang D S. A new constrained learning algorithm for function approximation by encoding a priori information into feed-forward neural networks. *Neural Computing & Applications*, 2008, 17(5–6): 433–439
  41. Boulanger R W, Idriss I M. *CPT and SPT Based Liquefaction Triggering Procedures*. Report No. UCD/CGM-14/01. Sacramento, CA: University of California, Davis, 2014
  42. Xie J F. Some opinions on modification of soil liquefaction evaluation method in seismic code. *Earthquake Engineering and Engineering Vibration*, 1984, 4(2): 95–109 (in Chinese)
  43. Juang C H. *Soil Liquefaction in the 1999 Chi-Chi, Taiwan, Earthquake*. Extracted from the website of Soil Liquefaction in the 1999 Chi-Chi, Taiwan, Earthquake. 2002
  44. Cetin K O, Youd T L, Seed R B, Bray J D, Stewart J P, Durgunoglu H T, Lettis W, Yilmaz M T. Liquefaction induced lateral spreading at Izmit Bay during the Kocaeli (Izmit)-Turkey Earthquake. *Journal of Geotechnical and Geoenvironmental Engineering*, 2004, 130(12): 1300–1313
  45. Sonmez B, Ulusay R, Sonmez H. A study on the identification of liquefaction-induced failures on ground surface based on the data from the 1999 Kocaeli and Chi-Chi earthquakes. *Engineering Geology*, 2008, 97(3–4): 112–125
  46. Li Z Y. *Research on the liquefaction evaluation method based on field investigations in the Bachu earthquake*. Harbin: Institution of Engineering Mechanics, 2012 (in Chinese)
  47. Li Z Y, Wang Y Z, Yuan X M. New CPT-based prediction method for soil liquefaction applicable to Bachu region of Xinjiang. *Chinese Journal of Geotechnical Engineering*, 2013, 35(1): 140–145 (in Chinese)
  48. Cox B R, Bachhuber J, Rathje E, Wood C M, Dulberg R, Kottke A, Green R A, Olson S M. Shear wave velocity- and geology-based seismic microzonation of Port-au-Prince, Haiti. *Earthquake Spectra*, 2011, 27(1\_suppl1): 67–92
  49. Green R A, Olson S M, Cox B R, Rix G J, Rathje E, Bachhuber J, French J, Lasley S, Martin N. Geotechnical aspects of failures at port-au-prince seaport during the 12 January 2010 Haiti earthquake. *Earthquake Spectra*, 2011, 27(1\_suppl1): 43–65
  50. Olson S M, Green R A, Lasley S, Martin N, Cox B R, Rathje E, Bachhuber J, French J. Documenting liquefaction and lateral spreading triggered by the 12 January 2010 Haiti earthquake. *Earthquake Spectra*, 2011, 27(1\_suppl1): 93–116

51. Kato K, Gonzalez D, Ledezma C, Ashford S. Analysis of pile foundations affected by liquefaction and lateral spreading with pinning effect during the 2010 Maule Chile earthquake. In: Proceedings of the 100th National Conference on Earthquake Engineering. Anchorage: Earthquake Engineering Research Institute, 2014
52. Kramer S L, Astaneh Asl B, Ozener P, Sideras S S. Perspectives on earthquake geotechnical engineering. *Geotechnical Geological and Earthquake Engineering*, 2015, 37: 285–309
53. Verdugo R, González J. Liquefaction-induced ground damages during the 2010 Chile earthquake. *Soil Dynamics and Earthquake Engineering*, 2015, 79: 280–295
54. Bhattacharya S, Hyodo M, Goda K, Tazoh T, Taylor C A. Liquefaction of soil in the Tokyo Bay area from the 2011 Tohoku (Japan) earthquake. *Soil Dynamics and Earthquake Engineering*, 2011, 31(11): 1618–1628
55. Ishihara K, Araki K, Bradley B. Characteristics of liquefaction-induced damage in the 2011 Great East Japan Earthquake. Christchurch: University of Canterbury, 2011
56. Sasaki Y, Towhata I, Miyamoto K, Shirato M, Narita A, Sasaki T, Sako S. Reconnaissance report on damage in and around river levees caused by the 2011 off the Pacific coast of Tohoku earthquake. *Soil and Foundation*, 2012, 52(5): 1016–1032
57. Ho T K. Random decision forests. In: Proceedings of the 3rd International Conference on Document Analysis and Recognition. Montreal: QC, 1995, 14–16
58. Zhang W G, Goh A T C. Multivariate adaptive regression splines for analysis of geotechnical engineering systems. *Computers and Geotechnics*, 2013, 48: 82–95
59. Ishibuchi H, Murata T. A multi-objective genetic local search algorithm and its application to flowshop scheduling. *IEEE Transactions on Systems, Man and Cybernetics. Part C, Applications and Reviews*, 1998, 28(3): 392–403
60. Li J, Cheng J, Shi J, Huang F. Brief Introduction of Back Propagation (BP) Neural Network Algorithm and Its Improvement. In: Proceedings of Advances in Intelligent and Soft Computing. Berlin: Springer, 2012
61. Silva F M, Almeida L B. Acceleration techniques for the back propagation algorithm. In: *Neural Networks. Lecture Notes in Computer Science*. Berlin: Springer, 1990
62. Chen G X. Research on reliability of liquefaction manifestation prediction. *Earthquake Engineering and Engineering Vibration*, 1991, 11(2): 85–96
63. Suliman A, Zhang Y. A review on back-propagation neural network in the application of remote sensing image classification. *Journal of Earth Science and Engineering*, 2015, 5: 52–65
64. Nawi N M, Atomi W H, Rehman M Z. The effect of data pre-processing on optimized training of artificial neural networks. *Procedia Technology*, 2013, 11: 32–39
65. Idriss I M, Boulanger R W. SPT-Based Liquefaction Triggering Procedures. Report No.UCD/CGM-10-02. Sacramento, CA: University of California, Davis, 2010
66. Seed H B, Idriss I M, Makdisi F, Banerjee N. Representation of irregular Stress Time Histories by Equivalent Uniform Stress Series in Liquefaction Analyses. No. EERC 75-29. Berkeley, SF: University of California, Berkeley, 1975
67. Idriss I M. An update to the Seed-Idriss simplified procedure for evaluating liquefaction potential. In: Proceedings of TRB Workshop on New Approaches to Liquefaction. Washington, D.C.: Transportation Research Board, 1999
68. Cetin K O, Seed R B, Der Kiureghian A K, Tokimatsu K, Harder J L F Jr, Kayen R E, Moss R E S. Standard penetration test-based probabilistic and deterministic assessment of seismic soil liquefaction potential. *Journal of Geotechnical and Geoenvironmental Engineering*, 2004, 130(12): 1314–1340
69. Boulanger R W. High overburden stress effects in liquefaction analyses. *Journal of Geotechnical and Geoenvironmental Engineering*, 2003, 129(12): 1071–1082
70. Liao S S C, Whitman R V. Overburden correction factors for SPT in sand. *Journal of Geotechnical Engineering*, 1986, 112(3): 373–377
71. Skempton A W. Standard penetration test procedures and the effects in sands of overburden pressure, relative density, particle size, aging and over consolidation. *Geotechnique*, 1986, 36(3): 425–447
72. Zhang J, Chen F Y, Juang C H, Chen Q. Developing joint distribution of  $a_{max}$  and  $M_w$  of seismic loading for performance-based assessment of liquefaction induced structural damage. *Engineering Geology*, 2018, 232: 1–11
73. Ministry of Housing and Urban-Rural Development of the People's Republic of China. Code for Seismic Design of Buildings, GB50011-2001. Beijing: China Building Industry Press, 2001 (in Chinese)
74. Ministry of Housing and Urban-Rural Development of the People's Republic of China. Code for Seismic Design of Buildings, GB50011-2010. Beijing: China Building Industry Press, 2016 (in Chinese)
75. Tokimatsu K, Yoshimi Y. Empirical correlation of soil liquefaction based on SPT-N values and fines content. *Soil and Foundation*, 1983, 23(4): 56–74
76. Youd T L, Idriss I M, Andrus R D, Arango I, Castro G, Christian J T, Dobry R, Finn W D L, Harder J L F Jr, Hynes M E, Ishihara K, Koester J P, Liao S C C, Marcuson W F III, Martin G R, Mitchell J K, Moriwaki Y, Power M S, Robertson P K, Seed R B, Stokoe K H II. Liquefaction resistance of soils: Summary report from the 1996 NCEER and 1998 NCEER/NSF workshops on evaluation of liquefaction resistance of soils. *Journal of Geotechnical and Geoenvironmental Engineering*, 2001, 127(10): 817–833
77. Hu J L, Tang X W, Qiu J N. Assessment of seismic liquefaction potential based on Bayesian network constructed from domain knowledge and history data. *Soil Dynamics and Earthquake Engineering*, 2016, 89: 49–60